INTERNATIONAL JOURNAL FOR NUMERICAL METHODS IN ENGINEERING
Int. J. Numer. Meth. Engng 2013; **93**:664–684
Published online 14 September 2012 in Wiley Online Library (wileyonlinelibrary.com). DOI: 10.1002/nme.4406

A variational multiscale method with subscales on the element boundaries for the Helmholtz equation

Joan Baiges[1,2,*,†] and Ramon Codina[1,2]

[1] *Universitat Politècnica de Catalunya, Jordi Girona 1-3, Edifici C1, 08034 Barcelona, Spain*
[2] *Centre Internacional de Mètodes Numèrics a l'Enginyeria (CIMNE), C/ Gran Capitán S/N 08034 Barcelona*

SUMMARY

In this paper, we apply the variational multiscale method with subgrid scales on the element boundaries to the problem of solving the Helmholtz equation with low-order finite elements. The expression for the subscales is obtained by imposing the continuity of fluxes across the interelement boundaries. The stabilization parameter is determined by performing a dispersion analysis, yielding the optimal values for the different discretizations and finite element mesh configurations. The performance of the method is compared with that of the standard Galerkin method and the classical Galerkin least-squares method with very satisfactory results. Some numerical examples illustrate the behavior of the method. Copyright © 2012 John Wiley & Sons, Ltd.

Received 11 October 2011; Revised 31 May 2012; Accepted 23 July 2012

KEY WORDS: Helmholtz equation; finite element methods; variational multiscale; stability

1. INTRODUCTION

The Helmholtz equation represents the propagation of acoustic and electromagnetic waves, which are two phenomena of great importance in many engineering problems. However, the solution of the Helmholtz equation by using the finite element method is subject to the so-called pollution error at high wave numbers, which causes the error of the numerical solution to grow very large and the frequency of the finite element solution to differ from the real solution to the problem. This results in the need of using relatively fine meshes if the standard Galerkin method is to be used. In this work, we present a new approach for coping with the pollution effect that can be easily added to standard finite element low-order implementations. This approach is based in the subscales on the element boundaries concept.

Several strategies have been devised to deal with the pollution effect. The Galerkin least-squares (GLS) method ([1–3]) deals with the pollution error by introducing the classical least-squares stabilization terms and defining the stabilization parameters by means of a dispersion analysis. However, the stabilization parameter is highly dependent on the direction of the wave propagation and the geometry of the finite element mesh. This turns out in relatively large errors for real problems, where the wave propagation direction is not known a priori.

Other approaches for dealing with the Helmholtz equation are the use of residual-free bubbles [4, 5], in which the finite element solution is enriched with functions that vanish on the element boundaries. In the strategy proposed in [6, 7], stabilizing terms on the basis of the residual of the finite element equations are employed. These residuals are taken both in the element interiors and in the element boundaries, which results in a formulation similar to the one proposed in this work.

*Correspondence to: Joan Baiges, Universitat Politècnica de Catalunya, Jordi Girona 1-3, Edifici C1, 08034 Barcelona, Spain.

†E-mail: jbaiges@cimne.upc.edu

However, the approach proposed in [7] cannot be included in a general framework such as the variational multiscale method (VMS). Another possibility for dealing with the Helmholtz equation is the use of discontinuous finite element methods [8]. This formulation shares with the one in the present work the fact that the stability of the method relies in stabilization terms defined on the element boundaries, but it requires discontinuous finite element spaces, which usually result in a higher number of degrees of freedom. Discontinuous Galerkin methods have also been used [9, 10]. Another family of methods is the discontinuous enrichment method (DEM) [11] (see [12, 13] for an application of the DEM to the Helmholtz equation), where the space for the fine scales (assuming that the solution is decomposed into a coarse scale and a fine scale) is allowed to be discontinuous, and particular spaces for the subscales are chosen depending on the problem to be solved. An additional Lagrange multiplier field is required in the DEM to impose weakly the continuity of the enrichment functions across the interelement boundaries. In the generalized finite element method, the fine scales are based in free-space solutions of the homogeneous differential equation, whereas conventional finite element functions are used for the coarse scales [14, 15]. A fourth-order compact scheme for the Helmholtz equation is developed in [16], although the method is specifically developed for structured meshes. See [17, 18] for an extensive review of existing approaches for solving the Helmholtz equation.

The approach we adopt for solving the Helmholtz equation is the VMS. In the VMS method, the solution is decomposed into a finite element part of the solution and a subgrid scale part. The subgrid part of the solution needs to be modeled, and the stabilizing terms of the formulation arise from this model for the subscales. The VMS method has previously been used to deal with the Helmholtz equation (see [19–22]). A common assumption in the VMS is to consider the subscales to vanish on the interlement boundaries. On the other hand, the contribution of the subscales on the interelement boundaries is taken into account in the method we propose. This approach has been successfully applied to the Stokes and Darcy problems in [23] and the problem of transmission conditions in fluids and solids [24] and is extended to the Helmholtz equation in this work. As we will see, taking into account the contribution of the boundary subgrid scales results in a method that is less dependent on the wave propagation direction than the classical approaches for linear and bilinear interpolations. However, the presented method turns out to be not well suited for higher order elements, in which nodes located in the middle of the element faces do not allow to devise a strategy for finding the optimal stabilization parameter.

The paper is organized as follows: the Helmholtz equation and a hybrid formulation for it are presented in Section 2, where additional unknowns for the traces and the fluxes are added to the formulation. The finite element approximation and the subscales on the element boundaries are introduced in Section 3. The optimal value for the stabilization parameters (obtained by means of a dispersion analysis) and a comparison with the classical GLS method for several finite element meshes and interpolations are presented in Section 4. Some numerical examples that illustrate the behavior of the proposed method and its application to aeroacoustics problems are presented in Section 5. Finally, some conclusions and remarks close the paper in Section 6.

2. PROBLEM STATEMENT

2.1. Helmholtz equation

Let us consider the boundary value problem:

$$\mathcal{L}u := -\Delta u - k^2 u = f \qquad \text{in } \Omega, \tag{1}$$

$$u = 0 \qquad \text{in } \Gamma_D, \tag{2}$$

$$\nabla u \cdot \mathbf{n} = \mathrm{i}ku + g \qquad \text{in } \Gamma_N, \tag{3}$$

where $\Omega \subset \mathbb{R}^d$ is a bounded domain, with $d = 2, 3$, $u : \Omega \longrightarrow \mathbb{C}$ is the unknown, $k > 0$ is the wave number, and f is the given source term.

DOI: 10.1002/nme

Let $V = H^1_\Gamma(\Omega) := \{v \in H^1(\Omega) \mid v = 0 \text{ on } \Gamma_D\}$. Let us define

$$B(u, v) := (\nabla u, \nabla v) - k^2(u, v), \tag{4}$$

$$L(v) := \langle f, v \rangle . \tag{5}$$

The variational form of the problem consists of finding $u \in V$ such that

$$B(u, v) - \langle v, \mathrm{i}ku \rangle_{\Gamma_N} = L(v) + \langle v, g \rangle_{\Gamma_N} \quad \forall v \in V. \tag{6}$$

Here and in the following, $(\cdot, \cdot)$ denotes the L^2 product in Ω. In general, the integral of two functions g_1 and g_2 over a domain ω will be denoted by $\langle g_1, g_2 \rangle_\omega$ and the norm in a function space X by $\| \cdot \|_X$, with the simplifications $\| \cdot \|_{L^2(\Omega)} \equiv \| \cdot \|$ and $\langle \cdot, \cdot \rangle_\Omega \equiv \langle \cdot, \cdot \rangle$. This symbol will also be used for the duality pairing.

2.2. *Hybrid formulation*

The numerical approximation we propose can be motivated from a hybrid formulation of the problem. Let us consider that $\bar{\Omega} = \bar{\Omega}_1 \cup \bar{\Omega}_2$, with $\Gamma = \partial\Omega_1 \cap \partial\Omega_2$ (see Figure 1).

Let now v_i, u_i be the restrictions of $u, v \in H^1_\Gamma$ to subdomain Ω_i, with v_i, u_i belonging to V_i, the subspace of $H^1(\Omega_i)$ of functions vanishing on Γ_D. Let us consider the trace of u on Γ, belonging to the space $T = H^{1/2}_{00}(\Gamma)$, and a flux corresponding to the differential operator associated to (6) belonging to the space $F_i = \left(H^{1/2}_{00}(\Gamma_i)\right)'$ (the prime denoting dual space). Then, the hybrid formulation of (6) that we consider is find $u_i \in H^1(\Omega_i)_\Gamma$, $\lambda_i \in F_i, i = 1, 2$ and $\gamma \in T$ such that

$$(\nabla u_1, \nabla v_1)_{\Omega_1} - k^2(u_1, v_1)_{\Omega_1} - \langle \lambda_1, v_1 \rangle_\Gamma - \langle v_1, \mathrm{i}ku_1 \rangle_{\Gamma_N} = \langle f, v_1 \rangle_{\Omega_1} + \langle v_1, g \rangle_{\Gamma_N} \quad \forall v_1 \in V_1, \tag{7}$$

$$(\nabla u_2, \nabla v_2)_{\Omega_2} - k^2(u_2, v_2)_{\Omega_2} - \langle \lambda_2, v_2 \rangle_\Gamma = \langle f, v_2 \rangle_{\Omega_2} \qquad \forall v_2 \in V_2, \tag{8}$$

$$\langle \mu_1, u_1 - \gamma \rangle_\Gamma = 0 \qquad \forall \mu_1 \in F_1, \tag{9}$$

$$\langle \mu_2, u_2 - \gamma \rangle_\Gamma = 0 \qquad \forall \mu_2 \in F_2, \tag{10}$$

$$\langle \kappa, \lambda_1 + \lambda_2 \rangle_\Gamma = 0 \qquad \forall \kappa \in T. \tag{11}$$

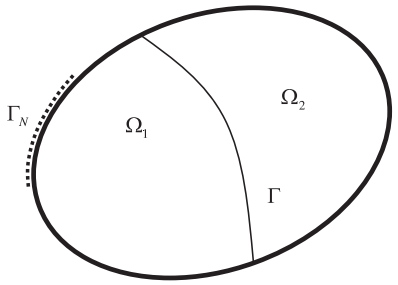

Figure 1. Splitting of the domain.

DOI: 10.1002/nme

If the solution of the continuous problem is smooth enough, the solution of the hybrid problem is $\gamma = u_1|_{\Gamma_1} = u_2|_{\Gamma_2}$, $\lambda_1 = -\lambda_2 = \boldsymbol{n}_1 \cdot \nabla u_1|_{\Gamma_1} = -\boldsymbol{n}_2 \cdot \nabla u_2|_{\Gamma_2}$.

2.3. Subgrid scales in the hybrid formulation

Let us consider a splitting of the space V of the form $V = \bar{V} \oplus \tilde{V}$. The component of u in $\bar{V}$ is considered as resolvable, whereas a closed form expression will be given for the component in $\tilde{V}$, the subgrid scale. Let V_i be also split as $V_i = \bar{V}_i \oplus \tilde{V}_i$, $i = 1, 2$. Any $u_i \in V_i$ can now be written as $u_i = \bar{u}_i + \tilde{u}_i$, with $\bar{u}_i \in \bar{V}_i$ and $\tilde{u}_i \in \tilde{V}_i$, we assume that $\bar{u}_1|_{\Gamma_1} = \bar{u}_2|_{\Gamma_2}$. Only the continuity for the component in $\tilde{V}_i$ needs to be enforced (weakly) through a variational equation.

Let us introduce the boundary operator

$$\mathcal{T}_i(\bar{v}_i) := \boldsymbol{n}_i \cdot \nabla \bar{v}_i|_{\Gamma_i},$$

where $v_i \in \bar{V}_i$, $i = 1, 2$. We may constrain the fluxes to be of the form $\lambda_i = \mathcal{T}_i(\bar{u}_i) + \tilde{\lambda}_i$, for appropriate $\tilde{\lambda}_i \in \tilde{F}_i$. Test functions in F_i can be similarly split as $\mu_i = \mathcal{T}_i(\bar{v}_i) + \tilde{\mu}_i$, with $\bar{v}_i \in \bar{V}_i$, $\tilde{\mu}_i \in \tilde{F}_i$. Finally, traces on boundaries can be split as $\gamma = \bar{u} + \tilde{\gamma}$ on Γ. On the intersecting boundary Γ, the restriction $\bar{u}$ is well defined because of the assumption $\bar{u}_1|_{\Gamma_1} = \bar{u}_2|_{\Gamma_2}$. Note that, in fact, $\tilde{F}_i = F_i$ and $\tilde{T} = T$. The tilde has been introduced to stress that we seek the subscale of fluxes and traces in these spaces.

Having introduced this decompositions and after some algebraic operations (see [23, 24] for a detailed explanation on these steps), we arrive to the final form of our hybrid formulation, which reads as follows: find $\bar{u}_i \in \bar{V}_i$, $\tilde{u}_i \in \tilde{V}_i$, $\tilde{\gamma} \in \tilde{T}$, $\tilde{\lambda}_i \in \tilde{F}_i$ $(i = 1, 2)$ such that

$$B(\bar{u}, \bar{v}) + \sum_{i=1}^{2} \langle \tilde{u}_i, \mathcal{L}_i(\bar{v}_i) \rangle_{\Omega_i} + \sum_{i=1}^{2} \langle \tilde{\gamma}, \mathcal{T}_i(\bar{v}_i) \rangle_{\Gamma} - \langle \bar{v}_1, \mathrm{i}k\bar{u}_1 \rangle_{\Gamma_N} = L(\bar{v}) + \langle \bar{v}_1, g \rangle_{\Gamma_N}, \tag{12}$$

$$\sum_{i=1}^{2} \langle \mathcal{L}_i(\bar{u}_i), \tilde{v}_i \rangle_{\Omega_i} + \sum_{i=1}^{2} B_i(\tilde{u}_i, \tilde{v}_i) - \sum_{i=1}^{2} \left\langle \tilde{\lambda}_i, \tilde{v}_i \right\rangle_{\Gamma} = \sum_{i=1}^{2} L_i(\tilde{v}_i), \tag{13}$$

$$\sum_{i=1}^{2} \left\langle \tilde{\kappa}, \mathcal{T}_i(\bar{u}_i) + \tilde{\lambda}_i \right\rangle_{\Gamma} = 0, \tag{14}$$

$$\sum_{i=1}^{2} \langle \tilde{\mu}_i, \tilde{\gamma} - \tilde{u}_i \rangle_{\Gamma} = 0, \tag{15}$$

for all $\bar{v}_i \in V_i$, $\tilde{v}_i \in \tilde{V}_i$, $\tilde{\kappa} \in \tilde{T}$, $\tilde{\mu}_i \in \tilde{F}_i$ $(i = 1, 2)$. This is the hybrid formulation on which we will base our finite element approximation.

3. FINITE ELEMENT APPROXIMATION

3.1. Scale splitting

Let $\mathcal{P}_h := \{K\}$ be a finite element partition of the domain Ω of size h and V_h a finite element space where an approximate solution $u_h \in V_h$ is sought. We assume that V_h is made *of continuous functions*, that is to say, V_h is conforming in V.

Consider the setting of the previous subsection with $\bar{V} = V_h$, and therefore $V = V_h \oplus \tilde{V}$, with $\tilde{V}$ to be defined, and $u = u_h + \tilde{u}$, $v = v_h + \tilde{v}$. The extension of (12)–(15) to multiple subdomains is straightforward. In particular, we will apply it considering each element a subdomain. No subscript will be used for the functions and operators in play to characterize the element domain over

DOI: 10.1002/nme

which they are defined, being this clear simply by the domain of integration. The discrete variational problem is to find $u_h \in V_h$, $\tilde{u} \in \tilde{V}$, $\tilde{\gamma} \in \tilde{T}$, and $\tilde{\lambda} \in \tilde{F}$ such that

$$B(u_h, v_h) + \sum_K \langle \tilde{u}, \mathcal{L}(v_h) \rangle_K + \sum_K \langle \tilde{\gamma}, \mathcal{T}(v_h) \rangle_{\partial K} - \langle v_h, \mathrm{i}k u_h \rangle_{\Gamma N} = L(v_h) + \langle v_h, g \rangle_{\Gamma_N}, \quad (16)$$

$$\sum_K \langle \mathcal{L}(u_h), \tilde{v} \rangle_K + \sum_K B_K(\tilde{u}, \tilde{v}) - \sum_K \left\langle \tilde{\lambda}, \tilde{v} \right\rangle_{\partial K} = \sum_K L_K(\tilde{v}), \quad (17)$$

$$\sum_K \left\langle \tilde{\kappa}, \mathcal{T}(u_h) + \tilde{\lambda} \right\rangle_{\partial K} + \langle \tilde{\kappa}, \mathrm{i}k u_h \rangle_{\Gamma_N} = \langle \tilde{\kappa}, g \rangle_{\Gamma_N}, \quad (18)$$

$$\sum_K \langle \tilde{\mu}, \tilde{\gamma} - \tilde{u} \rangle_{\partial K} = 0, \quad (19)$$

for all $\bar{v}_i \in V_i$, $\tilde{v}_i \in \tilde{V}_i$, $\tilde{\kappa} \in \tilde{T}$, $\tilde{\mu}_i \in \tilde{F}_i$, where $\tilde{T}$ is now the space of traces (of subscales) on the element boundaries (satisfying $\tilde{\gamma} = 0$ on $\partial\Omega$) and $\tilde{F}$ the space of fluxes on these boundaries.

Problems (16)–(19) are exact. The final approximation is obtained by choosing a way to approximate the subscales $\tilde{u}$, their traces on the element boundaries $\tilde{\gamma}$, and their fluxes $\tilde{\lambda}$. We explain how to do this in the following subsection.

3.2. Subscales on the element interiors

The approach we will follow for approximating the subscales on the element interiors corresponds to the orthogonal subscales stabilization method [25, 26]. As we will see, when this approach is applied to the Helmholtz equation and linear or bilinear finite element interpolations are used, the subscales vanish on the element interiors and $\tilde{u} = 0$ can be taken for this particular problem and interpolations.

To approximate $\tilde{u}$, we start by approximating (17) by integrating by parts,

$$\sum_K B_K(\tilde{u}, \tilde{v}) = -\sum_K \langle \Delta \tilde{u}, \tilde{v} \rangle_K + \sum_K \langle \boldsymbol{n} \cdot \nabla \tilde{u}, \tilde{v} \rangle_{\partial K} - k^2 \sum_K \langle \tilde{u}, \tilde{v} \rangle_K,$$

and assuming that $\boldsymbol{n} \cdot \nabla \tilde{u}$ cancels with the fluxes $\tilde{\lambda}$. The next step consists of using the approximation

$$\langle -\Delta \tilde{u}, \tilde{v} \rangle_K - k^2 \langle \tilde{u}, \tilde{v} \rangle_K \approx \tau^{-1} \langle \tilde{u}, \tilde{v} \rangle_K,$$

We will not justify this last step. It can be motivated, for example, by using an approximate Fourier analysis [25]. The subscales in the element interiors can now be expressed in terms of u_h from the equation

$$\sum_K \langle \mathcal{L}(u_h), \tilde{v} \rangle_K + \tau^{-1} \sum_K \langle \tilde{u}, \tilde{v} \rangle_K = \sum_K \langle f, \tilde{v} \rangle_K,$$

which can be described by saying the $\tilde{u}$ is the projection of the residual $f - \mathcal{L}(u_h)$ within each element multiplied by τ onto the space of subscales $\tilde{V}$. The most usual option is to take this projection as the identity. In the orthogonal subscales stabilization method, we take $\tilde{V}$ as the projection L^2-orthogonal to the finite element space V_h. This is equivalent to saying

$$\tilde{u} = \tau \tilde{P}(f - \mathcal{L}(u_h)),$$

where $\tilde{P}$ denotes the L^2 projection onto the space of subscales. But

$$\tilde{P}(f - \mathcal{L}(u_h)) = 0$$

for the Helmholtz equation if we take $\tilde{V}$ to be orthogonal to V_h, linear or bilinear elements are used, and $f \in V_h$. If f does not belong to V_h, that is, $\tilde{P}(f) \neq 0$, a consistency error is introduced, but

DOI: 10.1002/nme

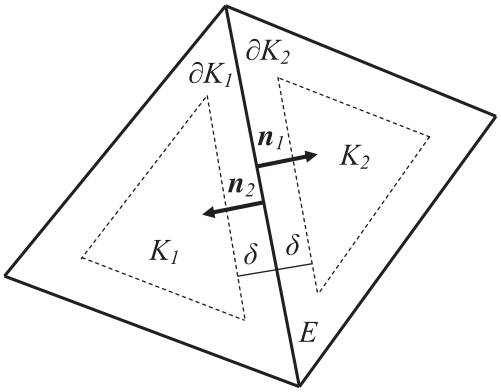

Figure 2. Notation for the approximation of the subscales on the element boundaries.

this error is optimally bounded (see [26]). Therefore, we can neglect the contribution of the interior subgrid scales for these particular interpolations. Summarizing, we take

$$\tilde{u} = 0, \tag{20}$$

in our variational formulation.

3.3. Subscales on the element boundaries

The way we propose to approximate the subscales was already presented in [23]. For completeness, we include it also here, where the approximation will be particularized for the Helmholtz equation. Let us consider for simplicity the 2D case and the situation depicted in Figure 2, where two elements K_1 and K_2 share an edge E (E stands for *edge* in two dimensions or face in three dimensions) . Let $\tilde{u}_i$ be the subscale approximated in the interior of element K_i, $i = 1, 2$. We assume that this approximation is valid up to a distance δ to the element boundary. This distance will be taken of the form

$$\delta = \delta_0 h_E, \tag{21}$$

with $0 \leqslant \delta_0 \leqslant 1/2$. h_E is a measure of the sizes of the elements connected by edge E and will be defined for each particular interpolation.

3.3.1. Approximation of $\tilde{\lambda}$. The values of $\tilde{\lambda}$ on ∂K are weak approximations to the fluxes of $\tilde{u}$. Given the trace $\tilde{\gamma}$ of this unknown, the following closed form expression for $\tilde{\lambda}$ is used:

$$\tilde{\lambda}_{\partial K_i \cap E} \approx \frac{\mu}{\delta}(\tilde{\gamma} - \tilde{u}_i), \quad i = 1, 2, \tag{22}$$

where now $\tilde{u}_i$ is the subscale computed in the element interiors and evaluated at edge E.

3.3.2. Approximation of $\tilde{\gamma}$. (18) states the weak continuity of the total fluxes on the element boundaries. The idea now is to replace this equation by an explicit prescription of this continuity.

Let $[\![\partial_n g]\!]_E = \boldsymbol{n}_1 \cdot \nabla g|_{\partial K_1 \cap E} + n_2 \cdot \nabla g|_{\partial K_2 \cap E}$ denote the jump of the normal derivative of a scalar function g across edge E. Suppose that E_0 is an interior edge. The condition to determine the expression of the subscale on the boundary is that the normal component of the fluxes be continuous across interelement boundaries. This can be written as follows:

$$0 = [\![\partial_n u]\!]_{E_0} \approx [\![\partial_n u_h]\!]_{E_0} + \tilde{\lambda}_{\partial K_1 \cap E_0} + \tilde{\lambda}_{\partial K_2 \cap E_0} \approx [\![\partial_n u_h]\!]_{E_0} + \frac{\mu}{\delta}\left(2\tilde{\gamma}_{E_0} - \tilde{u}_1 - \tilde{u}_2\right),$$

from where the approximation we propose is

$$\boxed{\tilde{\gamma}_{E_0} \approx \{\tilde{u}\}_{E_0} - \frac{\delta}{2}[\![\partial_n u_h]\!]_{E_0},} \tag{23}$$

DOI: 10.1002/nme

where $\{\tilde{u}\}_{E_0} := 1/2(\tilde{u}_1 + \tilde{u}_2)$ is the average of the subscales computed in the element interiors evaluated at edge E_0. δ_0 will play the role of a stabilization parameter for which we have a geometrical interpretation. From now onwards, we will use the symbol $=$ instead of $\approx$, understanding that in some places, we perform approximation (22) that has led us to (23).

3.4. Stabilized finite element problem

From the approximation of the fluxes (22), the expressions obtained for the traces (23), and the approximation for the subscales on the element interiors (20), one can obtain a problem for u_h alone. After some algebraic manipulations, the problem obtained is as follows: find $u_h \in V_h$ such that

$$B_{\text{stab}}(u_h, v_h) - \langle v_h, \mathrm{i}k u_h \rangle_{\Gamma_N} = L(v_h) + \langle v_h, g \rangle_{\Gamma_N} \quad \forall v_h \in V_h,$$

where

$$B_{\text{stab}}(u_h, v_h) = B(u_h, v_h) - \frac{\delta}{2} \sum_{E_0} \langle [\![\mathcal{T}(u_h)]\!], [\![\mathcal{T}(v_h)]\!] \rangle_{E_0}. \tag{24}$$

We must stress that the additional element boundary term in (24) increases the stencil of the final finite element matrix, reducing its sparsity. This is because this term involves the derivatives of test functions and nodal unknowns of neighbor elements, and as a consequence, the nodes belonging to these elements become connected. This can have a negative effect in the performance of the solver libraries used for solving the associated system of equations. This issue deserves further research, although it was not relevant in the numerical examples of this work, which were solved by using a direct solver.

4. DEFINITION OF δ_0 BY MEANS OF A DISPERSION ANALYSIS

As we have said, δ_0 plays the role of a stabilization parameter, with $0 \leqslant \delta_0 \leqslant 1/2$ according to the physical meaning of δ. To determine the optimal value for δ_0, we will perform a dispersion analysis that will be obtained from the finite element equations of an interior finite element node. This analysis will yield different optimal δ_0 for different finite element discretizations.

We must stress that stencil of the finite element mesh is incomplete near the boundary, which might lead to a different optimal value for the stabilization parameter in nodes close to the boundary. However, the additional edge stabilization terms are only added to the interior edges, which motivates us to use the stabilization parameter obtained from interior nodes. The fact that the stabilization parameter is determined only for an interior node has in practice very little or no effect in the performance of the method. This is illustrated in the numerical examples in Section 5, where no significant increase of the error can be appreciated in the boundary.

4.1. Dispersion analysis for linear finite elements

The exact solution for the Helmholtz equation (1) propagating without sources in the free space with constant wave number is a plane wave:

$$u = e^{\mathrm{i}\mathbf{k}\cdot\mathbf{x}}, \tag{25}$$

with $\mathbf{k} = k(\cos\theta, \sin\theta)^T$ and θ being the propagation direction.

When applied to solving the Helmholtz equation, the Galerkin method shows a high dependence on the anisotropy of the mesh. This is the reason why two different kind of meshes are considered in the case of linear elements. The optimal value for the stabilization parameter δ_0 will be obtained in each of these mesh types, and the behavior of the proposed method in these meshes will be compared with that of the Galerkin method and the classical stabilized GLS method. Let us start by considering the regular mesh in Figure 3, with element size h. The linear shape functions in the element coordinate system are

DOI: 10.1002/nme

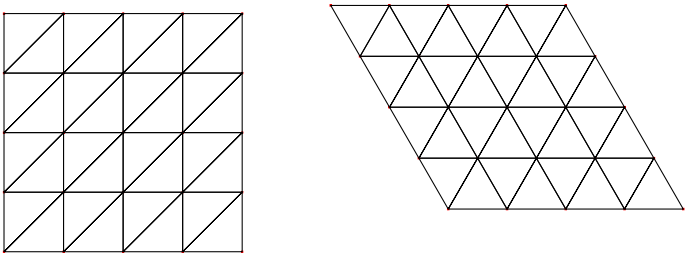

Figure 3. Regular and hexagonal meshes.

$$
\begin{aligned}
N_1 &= 1-\xi-\eta, \\
N_2 &= \xi, \\
N_3 &= \eta,
\end{aligned}
\tag{26}
$$

the nodal coordinates corresponding to $(\xi_1,\eta_1)=(0,0)$, $(\xi_2,\eta_2)=(1,0)$, and $(\xi_3,\eta_3)=(0,1)$. The definition of h_E in (21) is taken as

$$
h_E = \frac{h_i^2+h_j^2}{2l_{ij}}, \tag{27}
$$

where h_i stands for the size of element i. In the case of linear triangles, h is defined as two times the square root of the element area. l_{ij} stands for the length of the edge separating elements i and j. Note that (27) corresponds to dividing two times the mean value of the area of the neighbor elements by the length of the edge separating them. A similar expression involving the volume of the elements and the surface of the face separating them would correspond in the case of linear tetrahedra, although it has not been developed here. After introducing the linear interpolation shape functions in the stabilized form of the problem (24), assembling the contribution of the elements of the mesh, and substituting the nodally exact solution (25), we obtain the following discrete equation for a node interior to the finite element mesh:

$$
\begin{aligned}
0 = {} & 4 - 1/2(kh)^2 - 8\delta_0 - \left(1/6\,(kh)^2 - 2\delta_0\right)\cos\left((\cos\theta+\sin\theta)\,kh\right) \\
& - \left(2\ + 1/6(kh)^2 - 5\delta_0\right)\left(\cos(\sin\theta kh) + \cos(\cos\theta kh)\right) \\
& - \delta_0\ \cos\left((\cos\theta + 2\ \sin\theta)\,kh\right) - \delta_0\ \cos\left((2\ \cos\theta+\sin\theta)\,kh\right) \\
& - 2\,\delta_0\ \cos\left((\cos\theta-\sin\theta)\,kh\right).
\end{aligned}
\tag{28}
$$

See Figure 4 where the stencil of the additional boundary terms has been depicted. The order of the additional boundary stabilization terms is $\mathcal{O}(h^4)$ for this interpolation space and finite element mesh.

The optimal value for δ_0 is obtained by imposing that the previous equation is fulfilled. In the particular case of $\theta=0$, δ_0 reads:

$$
\boxed{\delta_0 = \frac{6-2(kh)^2-\cos(kh)(kh)^2-6\cos(kh)}{9-12\cos(kh)+3\cos(2kh)}.} \tag{29}
$$

An expression similar to (28) is found for the hexagonal mesh.

In the particular case of $\theta=0$, we obtain

$$
\delta_0 = \frac{a}{b}
$$

DOI: 10.1002/nme

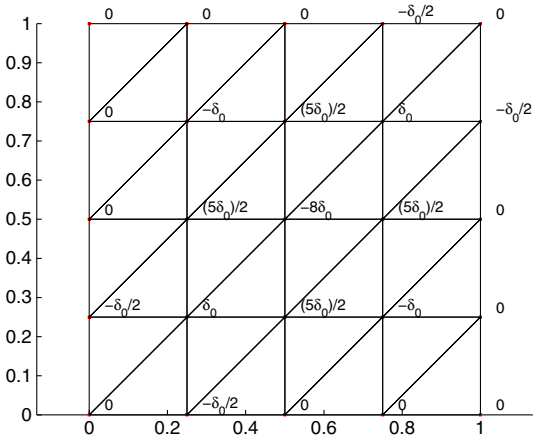

Figure 4. Stencil of the additional boundary terms for the structured linear triangle mesh, equation corresponding to the central node, real component.

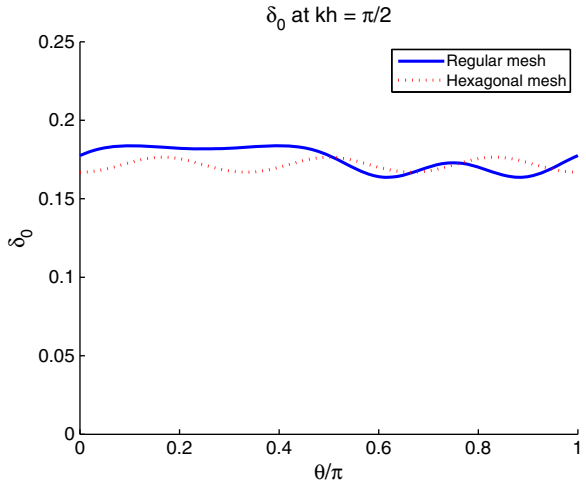

Figure 5. δ_0 as a function of θ for linear elements.

where

$$a = -36 + 3\sqrt{3}(kh)^2 + \left(24 + 2\sqrt{3}(kh)^2\right)\cos\left(2^{-1/2}3^{-1/4}kh\right) + \left(12 + \sqrt{3}(kh)^2\right)\cos\left(2^{1/2}3^{-1/4}kh\right)$$

$$b = -84 + 36\cos\left(2^{1/2}3^{-1/4}kh\right) + 72\cos\left(2^{-1/2}3^{-1/4}kh\right) - 24\cos\left(2^{-1/2}3^{3/4}kh\right).$$

δ_0 depends on the direction of the plane wave through θ. However, this dependence is small; Figure 5 shows the optimal values for δ_0 for different wave directions when $kh = \pi/2$. It can be observed that even for the regular mesh (which is anisotropic), the oscillations of δ_0 are small. This is an important feature of the method: when applied to real cases, the propagation direction of the wave will not be known a priori, and as a consequence, we need a method that behaves well independently of the direction of the wave and the type of mesh used. It is also interesting to observe the optimal value for δ_0 as a function of kh. As Figure 6 shows, this dependence is also small, δ_0 remaining practically constant at $\delta_0 \approx 16.8$ for the hexagonal mesh.

In the practical cases, we use $\delta_0(\theta = 0)$ in (29). Figure 7 shows the behavior of $\delta_0(\theta = 0)$ for $\theta = \pi/4$. The figure shows the recovered value for $k^h h$ in the finite element solution (which is computed by substituting the contribution from all the terms in the equation corresponding to

DOI: 10.1002/nme

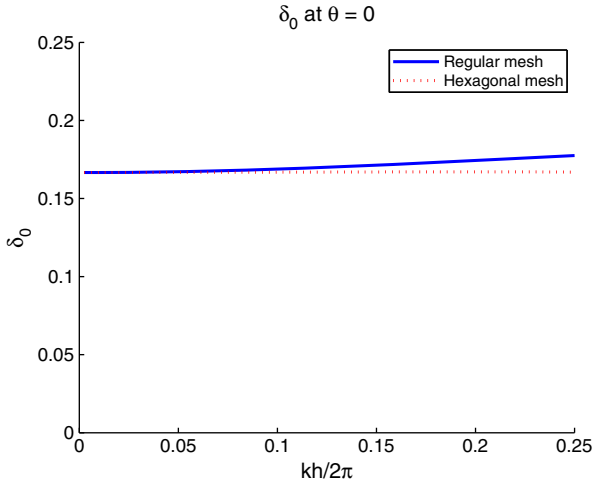

Figure 6. δ_0 as a function of kh for linear elements.

a central node of the finite element mesh) versus the value of the exact solution kh. The results for the proposed method are compared with those of the Galerkin method and the GLS method. We can see that very good results are obtained both for the regular mesh and the hexagonal mesh. In the case of the hexagonal mesh, the behavior of the proposed method is similar to that of the GLS method, the GLS method performing slightly better for large values of kh (very coarse finite element discretizations). However, the method we propose behaves much better compared with the GLS method when applied to non-isotropic meshes such as the regular mesh. The main advantage of the method we propose is this good behavior independent of the anisotropy of the mesh.

4.2. Dispersion analysis for bilinear finite elements

In this section, we perform the previous analysis in the case of bilinear finite elements. In this case, we consider the regular mesh depicted in Figure 8. The bilinear shape functions in the element coordinate system are

$$N_i(\xi,\eta) = \frac{(1+\xi_i\xi)(1+\eta_i\eta)}{4}, \qquad (30)$$
$$\xi_1 = \xi_3 = -1; \quad \xi_2 = \xi_4 = 1,$$
$$\eta_1 = \eta_2 = -1; \quad \eta_3 = \eta_4 = 1,$$

the nodal coordinates corresponding to $(\xi_1,\eta_1) = (-1,-1)$, $(\xi_2,\eta_2) = (1,-1)$, $(\xi_3,\eta_3) = (1,1)$, and $(\xi_4,\eta_4) = (-1,1)$. Again, the definition of h_E in (21) is taken as

$$h_E = \frac{h_i^2 + h_j^2}{2l_{ij}}, \qquad (31)$$

where h_i stands for the size of element i. In the case of bilinear finite elements, h is defined as the square root of the element area. l_{ij} stands for the length of the edge separating elements i and j. In this case, (31) corresponds to dividing the mean value of the area of the neighbor elements by the length of the edge separating them.

The optimal value for δ_0 is obtained as carried out in the previous section. See Figure 8 where the stencil of the additional stabilizing boundary terms has been depicted. Again, the order of the additional boundary stabilization terms is $\mathcal{O}(h^4)$ for the considered interpolation space and finite element mesh. In the particular case of $\theta = 0$, δ_0 reads

$$\boxed{\delta_0 = -\frac{((kh)^2+6)\cos(kh) + 2(kh)^2 - 6}{6(\cos(kh)-1)^2}.} \qquad (32)$$

DOI: 10.1002/nme

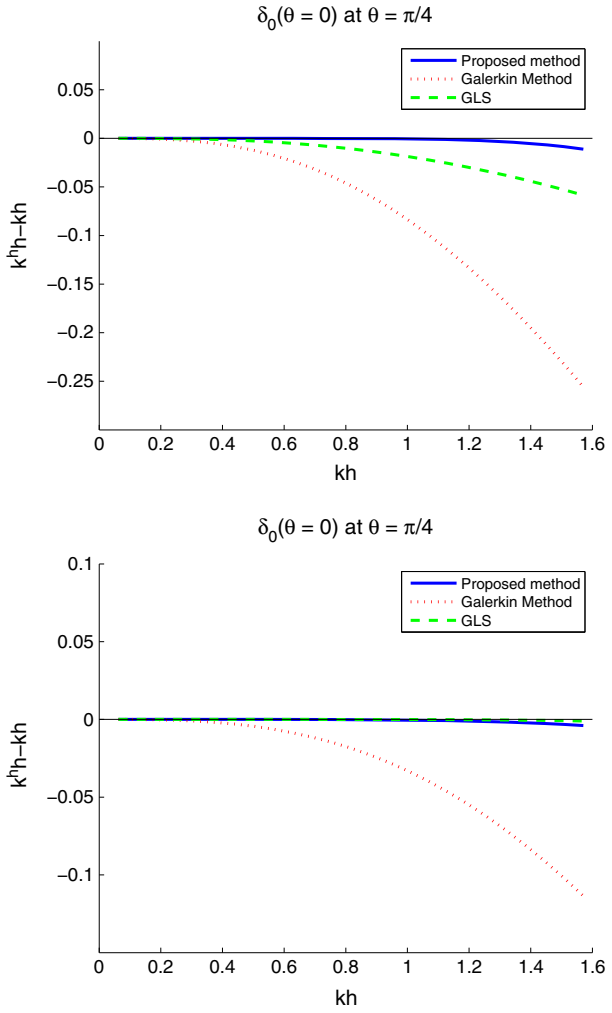

Figure 7. Behavior of $\delta_0(\theta = 0)$ at $\theta = \pi/4$ as a function of kh. Top: regular mesh. Bottom: hexagonal mesh.

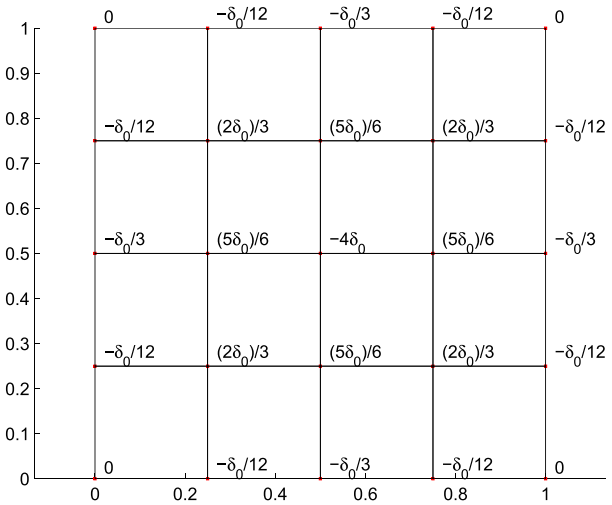

Figure 8. Stencil of the additional boundary terms for the structured bilinear quadrilateral mesh, equation corresponding to the central node, real component.

DOI: 10.1002/nme

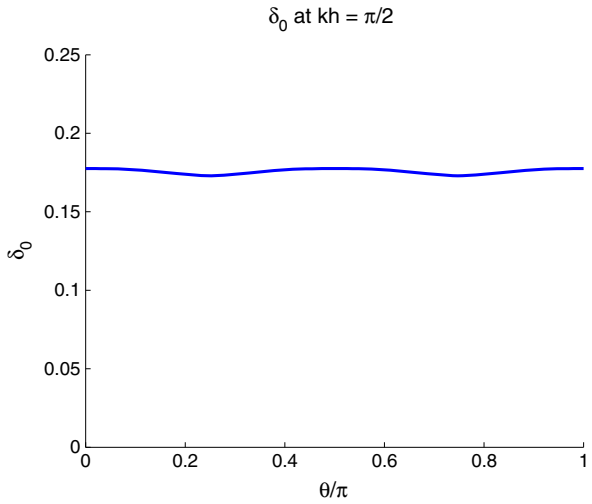

Figure 9. δ_0 as a function of θ for bilinear interpolations.

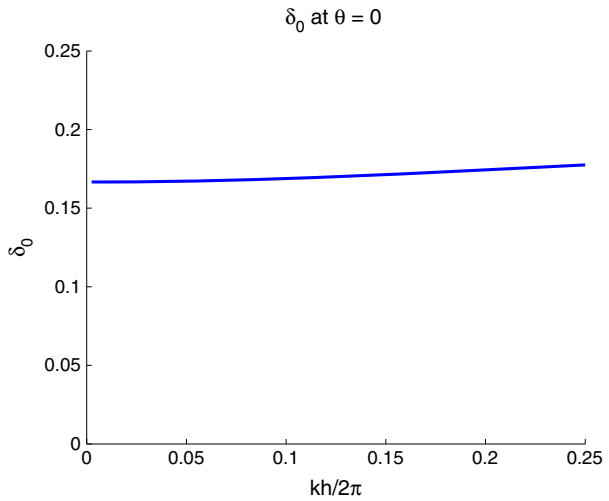

Figure 10. δ_0 as a function of kh for bilinear interpolations.

As in the case of linear elements, we are not interested in a method that is direction dependent, and we will rely on $\delta_0(\theta = 0)$. In the case of bilinear elements, the dependence of δ_0 on θ is even smaller than in the linear finite elements case. This is illustrated in Figure 9, where we can observe that δ_0 is practically constant against θ. We can also observe that values for δ_0 are very close to the ones obtained for linear interpolations, which allows us to assert that the dependence on the finite element interpolation is not too strong. The dependence of δ_0 with kh is also weak, as illustrated in Figure 10.

As in the case of linear elements, we will also rely on $\delta_0(\theta = 0)$ for the practical cases. In Figure 11, we show the recovered numerical value for $k^h h$ when $\theta = \pi/4$ and $\delta_0(\theta = 0)$ is used, and we compare it against the exact value for kh. The results for the proposed method are compared with those of the Galerkin method and the GLS method. Very little deviation from the exact value is observed in the case of bilinear interpolations. The method performs much better than the GLS or the standard Galerkin method, showing very little dependence on the anisotropy of the mesh and the wave propagation direction.

DOI: 10.1002/nme

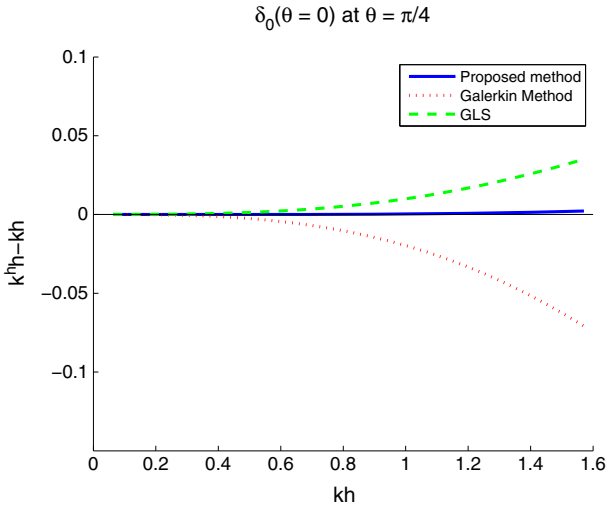

Figure 11. Behavior of $\delta_0(\theta = 0)$ at $\theta = \pi/4$ as a function of kh. Bilinear interpolation.

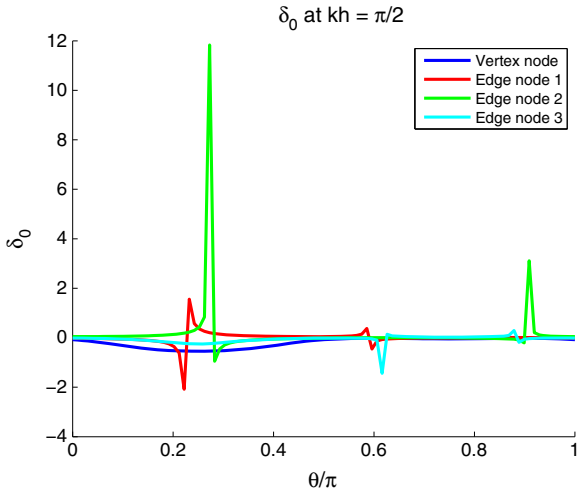

Figure 12. δ_0 as a function of θ for second order triangles.

4.3. Higher order elements

When repeating the previous dispersion analysis in the case of second-order triangles (with additional nodes on the center of the triangle edges), results are very dependent on the node the finite element test function is associated to and the propagation direction. In Figure 12, the optimal δ_0 as a function of θ is shown for a vertex node and each of the three edge nodes for a regular second-order triangle mesh. A very high dependence on the propagation direction is observed. This is associated to the fact that the contribution of the stabilization terms $\langle [\![\mathcal{T}(u_h)]\!], [\![\mathcal{T}(v_h)]\!] \rangle_{E_0}$ for an edge node vanishes for propagation directions that are parallel to the edge, and δ_0 should tend to infinity around this directions for the edge nodes to have zero dispersion error. In the case of vertex nodes (which are the only kind of nodes present in the case of linear triangles and bilinear quadrilaterals), this is not an issue because the node receives the contribution to $\langle [\![\mathcal{T}(u_h)]\!], [\![\mathcal{T}(v_h)]\!] \rangle_{E_0}$ from several non-parallel edges. This fact prevents the proposed method from being optimal for high-order finite elements with nodes in the center of the element faces. However, as shown in Section 5, very satisfactory results are obtained for low-order interpolations, which are the most widely used when solving the real-life engineering problems for which the method was designed.

DOI: 10.1002/nme

5. NUMERICAL EXAMPLES

In this section, we present some numerical examples that illustrate the behavior of the proposed method. In the first example, we solve the problem of a plane wave propagation, and we test the performance of the proposed method, the Galerkin, and GLS methods comparing the numerical results with the analytical solution. In the second example, the acoustics of the flow around a cylinder at low Reynolds number are solved, and results are compared with a reference numerical solution.

5.1. Plane wave propagation

The first example consists of a freely propagating two-dimensional plane wave. This problem consists of the following: find $u : \Omega \longrightarrow \mathbb{C}$ such that

$$-\Delta u - k^2 u = 0 \qquad \text{in } \Omega, \tag{33}$$

$$\nabla u \cdot \mathbf{n} = \mathrm{i}ku + g \qquad \text{in } \Gamma, \tag{34}$$

where $\Omega = [0, 1] \times [0, 1]$ and

$$g(\boldsymbol{x}) = \mathrm{i}k \left(1 + \boldsymbol{n} \cdot [\cos\theta, \sin\theta]^T\right) \exp\left(\mathrm{i}k \left(\boldsymbol{x} \cdot [\cos\theta, \sin\theta]^T\right)\right). \tag{35}$$

The exact solution for this problem is

$$u = \exp\left(\mathrm{i}k\boldsymbol{x} \cdot [\cos\theta, \sin\theta]^T\right).$$

We have solved this example using linear and bilinear finite element interpolation spaces, and we have compared the results obtained by using the proposed method with those of the Galerkin and GLS methods. The comparison has been performed for different mesh configurations.

In Figure 13, we compare the results obtained for a propagation direction of $\theta = \pi/4$ with a linear triangle hexagonal (unstructured) mesh using the Galerkin method, the GLS method, and the proposed method. In the case of the GLS method, we use the stabilization parameter for $\theta = \pi/8$, as recommended in [2]. In the case of the proposed method, we use the stabilization parameter corresponding to $\theta = 0$. We plot the imaginary part of the solution. We can observe that the best solution (no pollution error appreciable) is obtained with the proposed method. The GLS method performs quite well, although some oscillations can be observed in the right upper corner. Results are presented for $kh/(2\pi) = 0.2$, which corresponds to the limit case of five elements per wavelength. In Figure 14, we compare the performance of the methods in the case of a regular triangle mesh. In this case, the proposed method performs even better when compared with the GLS and Galerkin methods and shows no appreciable pollution error even in the case of this very coarse mesh.

In Figure 15, we compare the performance of the methods in the case of a bilinear regular mesh. Again, the GLS method performs quite well, although some pollution error can be observed in the upper right corner. In the solution for the proposed method, no pollution error is appreciated. As we will see, the error norm is also larger in the case of the GLS method. Similar results are obtained when comparing the performance on an unstructured bilinear finite element mesh (Figure 16).

In Table I, we can see the relative error obtained for the different meshes and stabilization methods. We can observe that the standard Galerkin method performs very poorly. The GLS method performs quite well for hexagonal unstructured triangular meshes, but results are inaccurate for regular meshes and bilinear finite elements. The method we propose clearly outperforms the standard Galerkin method and the GLS method in all the studied cases, independently of the finite element space or the mesh discretization.

5.2. Sound propagation for the aeolian tone generated by the incompressible flow around a cylinder

In this numerical example, we simulate the propagation of sound generated by an incompressible flow around a cylinder. The source term for the Helmholtz equation is obtained by numerically simulating the incompressible Navier–Stokes equations around a cylinder and computing the acoustic

DOI: 10.1002/nme

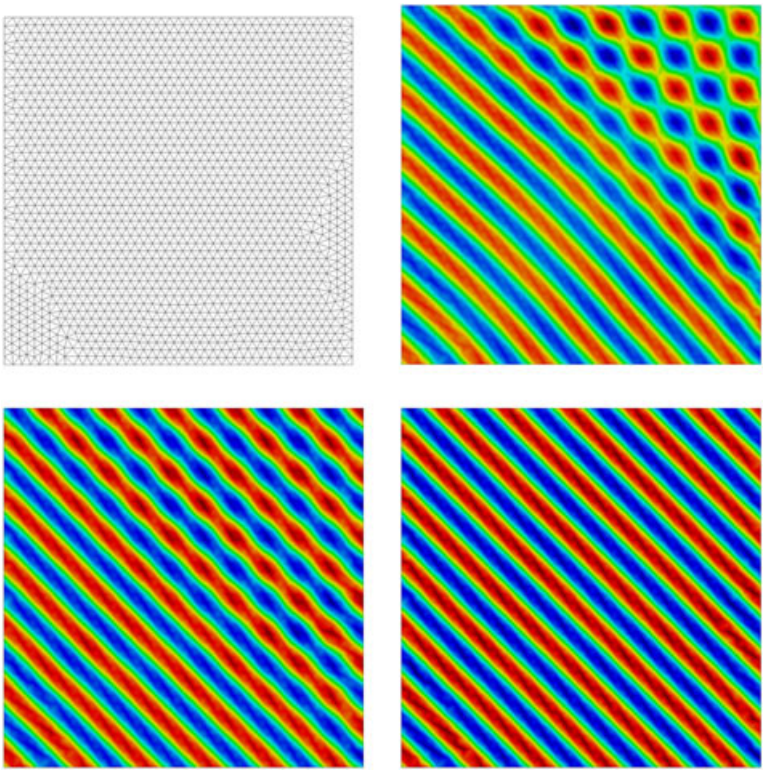

Figure 13. Hexagonal mesh and solution for the Galerkin (top right), Galerkin least squares (bottom left), and proposed methods (bottom right), $kh/(2\pi) = 0.2$.

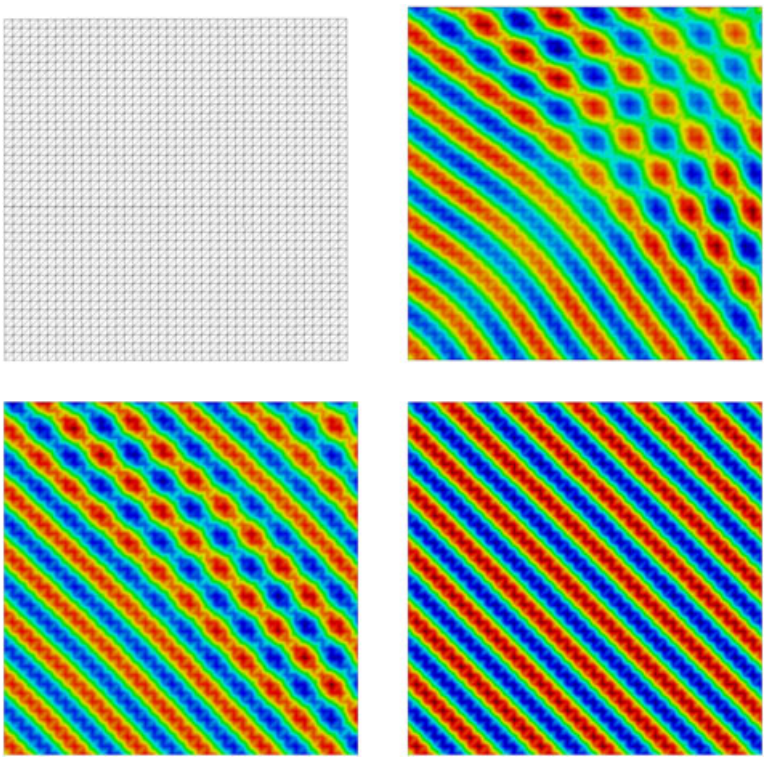

Figure 14. Regular mesh and solution for the Galerkin (top right), Galerkin least squares (bottom left), and proposed methods (bottom right), $kh/(2\pi) = 0.2$.

DOI: 10.1002/nme

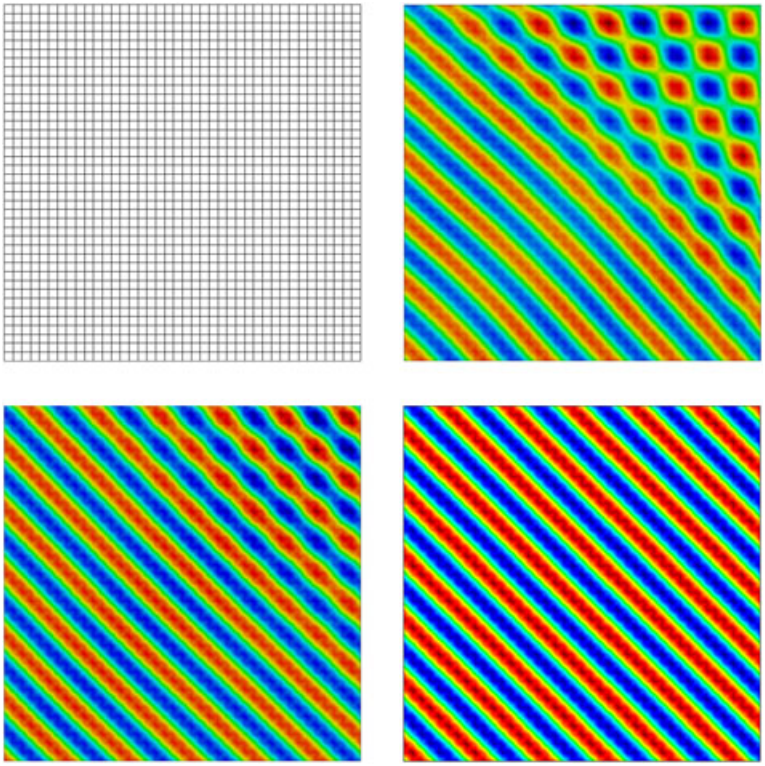

Figure 15. Bilinear mesh and solution for the Galerkin (top right), Galerkin least squares (bottom left), and proposed methods (bottom right), $kh/(2\pi) = 0.2$.

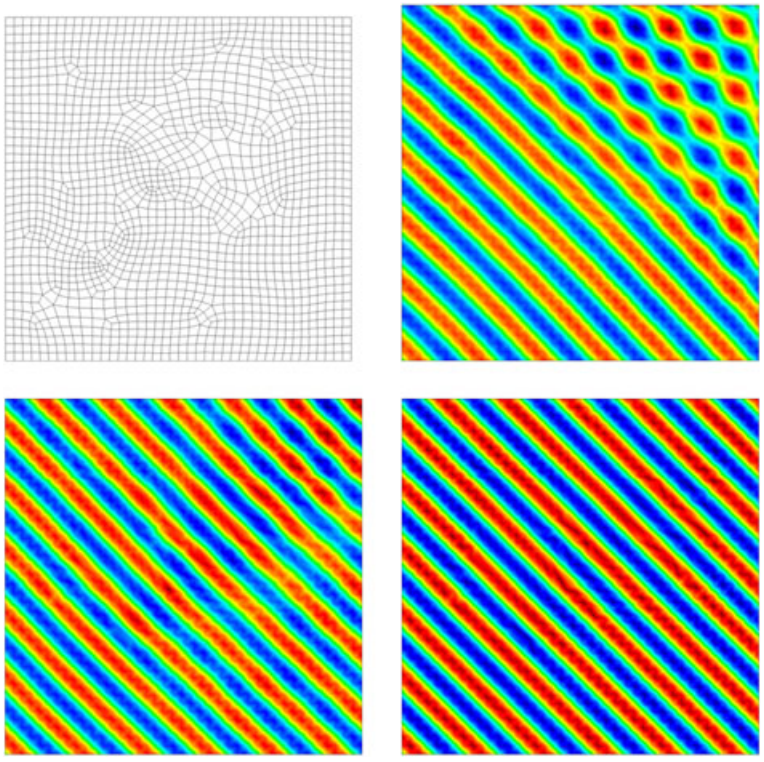

Figure 16. Unstructured bilinear mesh and solution for the Galerkin (top right), Galerkin least squares (bottom left), and proposed methods (bottom right), $kh/(2\pi) = 0.2$.

DOI: 10.1002/nme

Table I. Relative error $||u - u_h||/||u||$.

	Linear hexagonal	Linear regular	Bilinear regular	Bilinear unstructured
Galerkin	1.055	1.277	0.78	0.76
Galerkin least squares	0.181	0.681	0.424	0.466
Proposed method	0.045	0.129	0.026	0.031

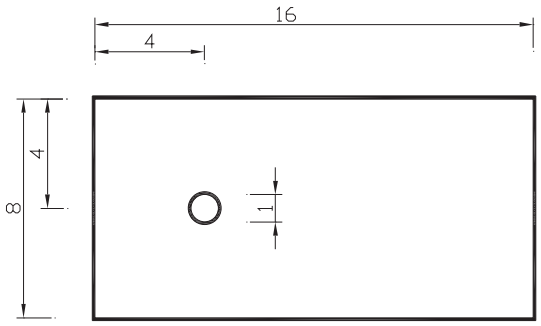

Figure 17. Computational domain for the incompressible flow around a cylinder problem.

source terms by using Lighthill's analogy (see [27, 28]). The numerical example we present corresponds to the direct numerical simulation presented in [29]. The accuracy of the obtained solution relies both on the accuracy of the simulation of the flow equations and the accuracy of the solution of the Helmholtz equation, for which we have proposed our novel numerical method.

The incompressible Navier–Stokes equations consist in finding a velocity field $\boldsymbol{u}$ and a pressure p such that

$$\partial_t \boldsymbol{u} + \boldsymbol{u} \cdot \nabla \boldsymbol{u} - \nu \Delta \boldsymbol{u} + \nabla p = \boldsymbol{f},$$
$$\nabla \cdot \boldsymbol{u} = 0,$$

in Ω and for $t > 0$, where $\boldsymbol{f}$ is the vector of body forces and ν the kinematic viscosity. Appropriate initial and boundary conditions have to be appended to this problem. To solve it, we use a numerical scheme which, as the method proposed in this paper for the Helmholtz equation, is based on the VMS. Our approach for solving the Navier–Stokes equations is extensively explained in [30]. The use of this numerically stable approach allows us to circumvent both the instabilities because of the convective term and the inf–sup condition because of the incompressibility constraint. As a consequence, we are able to use equal-order interpolations for the velocity and the pressure variables.

The domain where the flow around the cylinder is computed is depicted in Figure 17. The entry velocity is set to 0.2. On the cylinder, surface velocity is prescribed to 0, and slip boundary conditions are applied in the upper and lower walls of the domain. In the exit boundary, we prescribe the normal component of the traction to be 0. The viscosity is set to $\nu = 0.00133$. The Reynolds number refers to the size of the cylinder that is $Re = 150$. A 181,513 linear triangle mesh with strong refinement around the cylinder is used. The time step is set to $\delta t = 1.5$.

In Figure 18 (left), we depict the velocity field after the flow has developed. In the right, we have plotted the vertical velocity Fourier transform. This plot shows that the main oscillation frequency is at $f = 0.035$. We will study the sound propagation for this particular frequency. In Figure 19, we depict the Fourier transform of the source term at $f = 0.035$. We can observe that the sound generation occurs in the wake behind the cylinder and the upstream boundary layer. The intensity of the sound source diminishes quickly as we move away from the cylinder.

The computational domain used to solve the Helmholtz equation consists of a circular crown domain of exterior radius $R = 300$. The radius of the interior cylinder is again $r = 0.5$ and coincides with the cylinder of the Navier–Stokes equations domain. This problem consists of the following:

DOI: 10.1002/nme

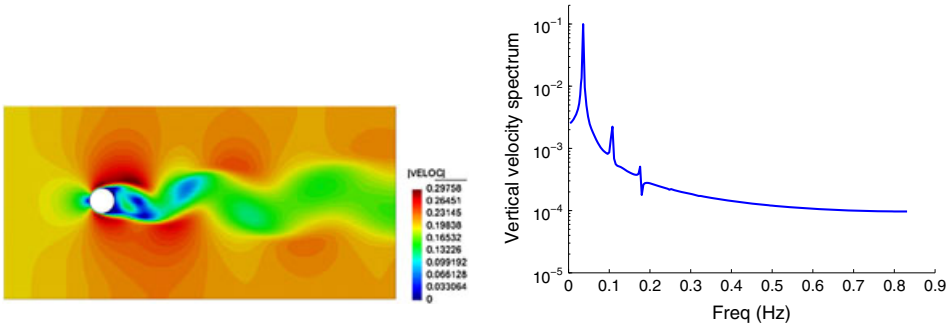

Figure 18. Results for the incompressible flow around the cylinder.

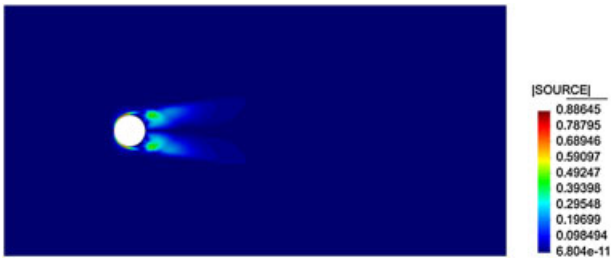

Figure 19. Source term distribution at $f = 0.035$.

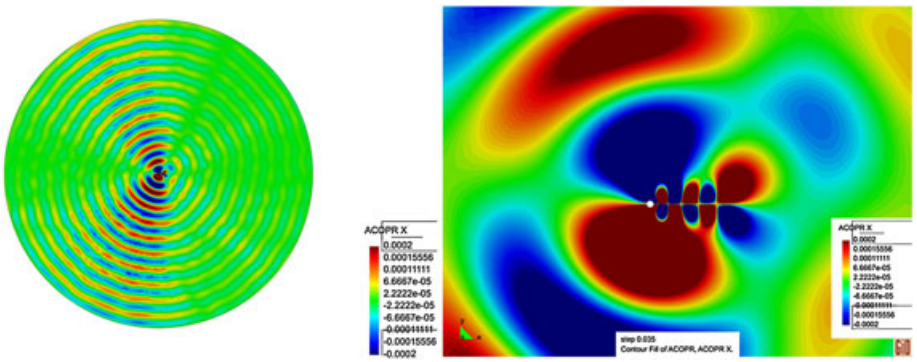

Figure 20. Real part of the solution for the complete computational domain (left) and detail around the cylinder (right).

find $u : \Omega \longrightarrow \mathbb{C}$ such that

$$-\Delta u - k^2 u = 0 \qquad \text{in } \Omega, \tag{36}$$

$$\nabla u \cdot \mathbf{n} = \mathrm{i}ku \qquad \text{in } \Gamma_E, \tag{37}$$

$$\nabla u \cdot \mathbf{n} = 0 \qquad \text{in } \Gamma_I, \tag{38}$$

where Γ_E corresponds to the exterior boundary and Γ_I corresponds to the interior boundary. The wave number is taken as $k = 2\pi f/c$, where $f = 0.035$ corresponds to the main oscillation frequency and $c = 1$ is the speed of sound.

In Figure 20, we show the real part of the solution for the Helmholtz equation. A dipole pattern can be observed in the far field that is generated by the lift fluctuations on the cylinder. The effect of the vortices in the wake of the cylinder can also be observed. However, because of the symmetry of the problem, these vortices cancel each other and have little effect on the global propagation of the solution.

DOI: 10.1002/nme

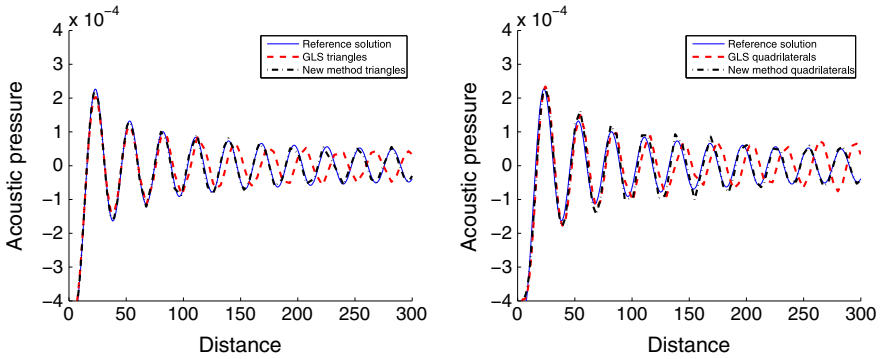

Figure 21. Comparison between the reference and coarse mesh solutions for the Galerkin least squares (GLS) and the proposed methods. Left: triangular elements. Right: quadrilateral elements.

In Figure 21, we compare the performance of the proposed method against the GLS method. The reference solution corresponds to the solution obtained by using the GLS method in a fine triangular mesh (695, 208 elements). The coarse mesh where we test the GLS method and the new method consists of 43, 482 elements in the case of linear triangles and 26, 723 elements in the case of bilinear quadrilaterals. The fine mesh has an element size of 30 elements per wavelength, whereas in the case of the coarse meshes, the element size is of five elements per wavelength. In both the coarse and fine meshes, some refinement is done in the area close to the cylinder so that the source term can be correctly represented by the finite element functions. We can appreciate that little deviation is observed between the reference solution and the coarse mesh solution for the new method, even for the limit case of five elements per wavelength. On the other hand, the GLS method suffers from pollution error, which translates into a phase error, clearly appreciable in the exterior boundary of the computational domain.

6. CONCLUSIONS

In this paper, we have presented a new method for dealing with the pollution effect when solving the Helmholtz equation with low-order finite elements. The presented approach is based on the VMS, and its main feature consists of taking into account the contribution of the subscales on the element boundaries. The expression for the subscales on the element boundaries is obtained by introducing a hybrid formulation and imposing the continuity of tractions across the interelement boundaries.

The value of the interelement boundary stabilization parameter δ_0 is determined by doing a dispersion analysis and imposing that the exact solution for a freely propagating plane wave is recovered for the proposed numerical scheme. The optimal value for the stabilization parameter depends both on the anisotropy of the mesh and the wave direction, but, contrary to other methods for dealing with the pollution effect, this dependence is small. This results in a stabilization parameter that can be taken independent of the propagation direction. Linear and bilinear finite element interpolations are studied, and the optimal value for the stabilization parameter is obtained for each of them, the numerical scheme also showing little dependence on the finite element interpolation. However, it is not possible to obtain a direction-independent stability parameter for higher order elements, and the method turns out to be suitable only for linear and bilinear interpolations.

The performance of the method is tested in several numerical examples, where the obtained results are compared with those of the standard Galerkin method and the classical GLS method. The proposed method produces very accurate results and clearly outperforms the GLS method. Moreover, results show very little dependence on the finite element mesh employed and the wave propagation direction, and the resulting formulation is easy to implement because it only involves an additional integral in the interelement boundaries.

DOI: 10.1002/nme

ACKNOWLEDGEMENT

The authors gratefully acknowledge the financial support from EU FP7 VALIANT Project(ACP8-GA-2009-233680).

REFERENCES

1. Harari I, Hughes TJR. Galerkin/least-squares finite element methods for the reduced wave equation with non-reflecting boundary conditions in unbounded domains. *Computer Methods in Applied Mechanics and Engineering* 1992; **98**(3):411–454.
2. Harari I, Nogueira CL. Reducing dispersion of linear triangular elements for the Helmholtz equation. *Journal of Engineering Mechanics* 2002; **128**:351–358.
3. Thompson LL, Pinsky PM. A Galerkin least-squares finite element method for the two-dimensional Helmholtz equation. *International Journal for Numerical Methods in Engineering* 1995; **38**(3):371–397.
4. Franca LP, Farhat C, Macedo AP, Lesoinne M. Residual free bubbles for the Helmholtz equation. *International Journal for Numerical Methods in Engineering* 1997; **40**(21):4003–4009.
5. Franca LP, Macedo AP. A two-level finite element method and its application to the Helmholtz equation. *International Journal for Numerical Methods in Engineering* 1998; **43**:23–32.
6. Oberai AA, Pinsky PM. A numerical comparison of finite element methods for the Helmholtz equation. *Journal of Computational Acoustics* 2000; **8**:211–221.
7. Oberai AA, Pinsky PM. A residual-based finite element method for the Helmholtz equation. *International Journal for Numerical Methods in Engineering* 2000; **49**:399–419.
8. Alvarez GB, Loula AFD, do Carmo EGD, Rochinha FA. A discontinuous finite element formulation for Helmholtz equation. *Computer Methods in Applied Mechanics and Engineering* 2006; **195**:4018–4035.
9. Farhat C, Harari I, Hetmaniuk U. A discontinuous Galerkin method with Lagrange multipliers for the solution of the Helmholtz problems in the mid-frequency regime. *Computer Methods in Applied Mechanics and Engineering* 2003; **192**:1389–1419.
10. Farhat C, Tezaur R, Weidemann-Gorian P. Higher order extensions of a discontinuous Galerkin method for mid-frequency Helmholtz problems. *International Journal for Numerical Methods in Engineering* 2004; **61**:1938–1956.
11. Farhat C, Harari I, Franca LP. The discontinuous enrichment method. *Computer Methods in Applied Mechanics and Engineering* 2001; **192**:3195–3209.
12. Farhat C, Harari I, Hetmaniuk U. The discontinuous enrichment method for multiscale analysis. *Computer Methods in Applied Mechanics and Engineering* 2003; **192**:3195–3209.
13. Grosu E, Harari I. Three dimensional element configurations for the discontinuous enrichment method for acoustics. *International Journal for Numerical Methods in Engineering* 2009; **78**:1261–1291.
14. Stroubolis T, Babuška I, Copps K. The design and analysis of the generalized finite element method. *Computer Methods in Applied Mechanics and Engineering* 2000; **181**:43–69.
15. Stroubolis T, Babuška I, Hidajat R. The generalized finite element method for Helmholtz equation: theory, computation, and open problems. *Computer Methods in Applied Mechanics and Engineering* 2006; **195**:4711–4731.
16. Nadukandi P, Oñate E, Garcia J. A fourth-order compact scheme for the Helmholtz equation: alpha-interpolation of FEM and FDM stencils. *International Journal for Numerical Methods in Engineering* 2011; **86**:18–46.
17. Harari I. Multiscale finite elements for acoustics: continuous, discontinuous, and stabilized methods. *International Journal for Numerical Methods in Engineering* 2008; **6**(6):511–531.
18. Thomson LL. A review of finite-element methods for time-harmonic acoustics. *Journal of the Acoustical Society of America* 2006; **119**:1315–1330.
19. Guasch O, Codina R. An algebraic subgrid scale finite element method for the convected Helmholtz equation in two dimensions with applications in aeroacoustics. *Computer Methods in Applied Mechanics and Engineering* 2007; **196**:4672–4689.
20. Guasch O, Codina R. Computational aeroacoustics of viscous low speed flows using subgrid scale finite element methods. *Journal of Computational Acoustics* 2009; **17**:309–330.
21. Hughes TJR. Multiscale phenomena: Green's function, the Dirichlet-to-Neumann formulation, subgrid scale models, bubbles and the origins of stabilized formulations. *Computer Methods in Applied Mechanics and Engineering* 1995; **127**:387–401.
22. Oberai AA, Pinsky PM. A multiscale finite element method for the Helmholtz equation. *Computer Methods in Applied Mechanics and Engineering* 1998; **154**(3-4):281–297.
23. Codina R, Principe J, Baiges J. Subscales on the element boundaries in the variational two-scale finite element method. *Computer Methods in Applied Mechanics and Engineering* 2009; **198**:838–852.
24. Codina R, Baiges J. Finite element approximation of transmission conditions in fluids and solids introducing boundary subgrid scales. *International Journal for Numerical Methods in Engineering* 2011; **87**:386–411.
25. Codina R. Stabilized finite element approximation of transient incompressible flows using orthogonal subscales. *Computer Methods in Applied Mechanics and Engineering* 2002; **191**:4295–4321.
26. Codina R. Analysis of a stabilized finite element approximation of the Oseen equations using orthogonal subscales. *Applied Numerical Mathematics* 2008; **58**:264–283.

DOI: 10.1002/nme

27. Lighthill M. On sound generated aerodinamically I. General theory. *Proc. R. Soc. Lond.*, 1952; 211 A:1107:564–587.
28. Lighthill M. On sound generated aerodinamically II. Turbulence as a source of sound. *Proceeding of the Royal Society of London*, 1954; 222 A:1148:1–32.
29. Inoue O, Hatakeyama N. Sound generation by a two-dimensional circular cylinder in a uniform flow. *Journal of Fluid Mechanics* 2002; **471**:285–314.
30. Codina R. A stabilized finite element method for generalized stationary incompressible flows. *Computer Methods in Applied Mechanics and Engineering* 2001; **190**:2681–2706.

DOI: 10.1002/nme